ADVANCED FUNCTIONAL MATERIALS



DOI: 10.1002/adfm.200800321

# Charged Rod-Like Nanoparticles Assisting Single-Walled Carbon Nanotube Dispersion in Water**

By *Changwoo Doe, Sung-Min Choi,* Steven R. Kline, Hyung-Sik Jang,* and *Tae-Hwan Kim*

A new dispersant for stabilization of single wall carbon nanotubes (SWNTs) in water that simultaneously utilizes three different dispersion or stabilization mechanisms: surfactant adsorption, polymeric wrapping, and Coulomb repulsive interaction, has been demonstrated. The new dispersant, a charged rod-like nanoparticle (cROD), is a cylindrical micelle wrapped by negatively charged polymers which is fabricated by the aqueous free radical polymerization of a polymerizable cationic surfactant, cetyltrimethylammonium 4-vinylbenzoate (CTVB), in the presence of sodium 4-styrenesulfonate (NaSS). The surface charge density of the cRODs is controlled by varying the concentration of NaSS. Dispersions of SWNTs are obtained by sonicating a mixture of SWNTs and cROD in water, followed by ultra-centrifugation and decanting. While the cRODs with neutral or low surface change densities (0 and 5 mol % NaSS) result in very low dispersion power and poor stability, the cRODs with high surface charge densities (15, 25, and 40 mol % NaSS) produce excellent dispersions with SWNT concentration as high as 437 mg $L^{-1}$ and long term stability. The sharp van Hove transition peaks of the cROD assisted SWNT dispersions indicate the presence of individually isolated SWNTs. Atomic force microscopy and small angle neutron scattering analysis show that the dominant encapsulation structure of the cROD assisted SWNTs is surfactant assisted polymeric wrapping. SWNTs dispersed by the cRODs can be fully dried and easily re-dispersed in water, providing enhanced processibility of SWNTs.

## 1. Introduction

Single-wall carbon nanotubes (SWNTs) exhibit remarkable physical properties[1–3] that make the nanotubes excellent candidates for a variety of potential applications such as nanoscale electronic[4,5] and quantum devices,[6] and biosensors[7,8] as well as reinforcement for materials.[9,10] Despite such extraordinary properties of SWNTs, there are still many issues to be resolved for their practical application. Two of the key issues are the insolubility and bundling of SWNTs in aqueous solution due to their strong hydrophobicity[11,12] and van der Waals attractions,[13] which make the solution processing of SWNTs for practical applications very problematic. In recent years, progress has been made in preparing dispersions of individually isolated SWNTs in aqueous media using various dispersants such as surfactants,[14–17] polymers,[11,18–20] lipids,[21–23] or DNAs.[24,25] Typically, the SWNTs are exfoliated from bundles by sonication and encapsulated by dispersants, eliminating or minimizing the interface between the hydrophobic surface of SWNTs and the aqueous medium. The underlying mechanisms of the encapsulation can vary depending on the chemical or physical properties of the dispersants. For example, the amphiphilicity of surfactants drive them to form a self-assembled sheath on the hydrophobic surface of SWNTs in aqueous solution and the long chain length and flexibility of polymers provide efficient wrapping around SWNTs. Generally, charged molecules as dispersants are advantageous, enhancing the stability of SWNT dispersions by providing repulsive Coulomb interactions between encapsulated SWNTs. The nucleobases, long chain length and flexibility, and positive charge of DNAs make them good dispersants utilizing π-stacking, wrapping, and electrostatic repulsion simultaneously.

While there have been many studies of dispersions of SWNTs in aqueous solutions as mentioned above, more effective preparations of SWNT dispersions in aqueous solutions are still of great interest for applications. A SWNT dispersion technique that can utilize the advantages of different types of dispersants simultaneously would provide synergistic enhancement of SWNT dispersion. While there have been a few reports which discuss the possible synergistic enhancement of SWNT dispersion in water,[26,27] it has not been fully exploited yet. In this work, we report a new

[*] Prof. S.-M. Choi, C. Doe, H.-S. Jang, and T.-H. Kim
Department of Nuclear and Quantum Engineering
Korea Advanced Institute of Science and Technology
373-1 Guseong-dong, Yuseong-gu, Daejeon 305-701
(Republic of Korea)
E-mail: sungmin@kaist.ac.kr
Dr. S. R. Kline
NIST Center for Neutron Research
Gaithersburg, MD 20899-6102 (USA)

[**] This work is supported by the Ministry of Education, Science and Technology of Korea through the Basic Atomic Energy Research Institute (BAERI) program, the basic science research program (R-01-2008-000-10219-0) and the CNRF project. This work utilized facilities supported in part by the National Science Foundation (DMR-9986442). The mention of commercial products does not imply endorsement by NIST, nor does it imply that the materials or equipment identified are necessarily the best available for the purpose. Supporting Information is available online from Wiley InterScience or from the authors.

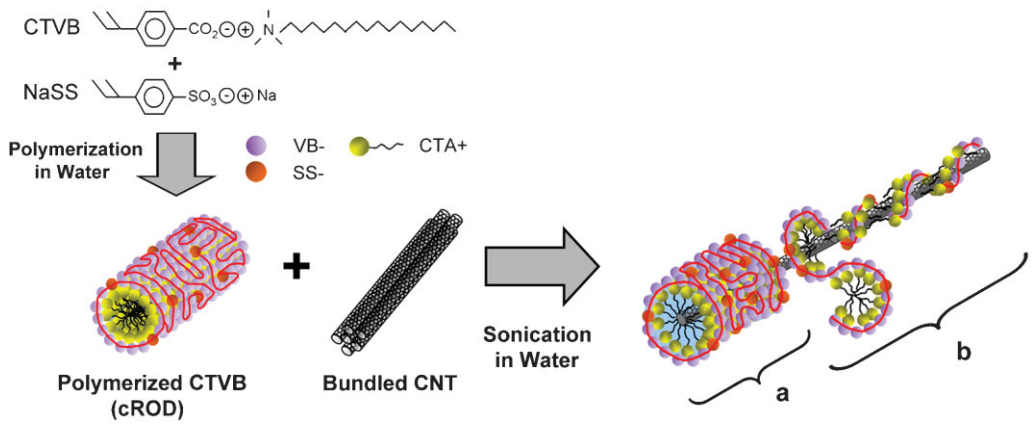


**Figure 1.** Schematic diagram of SWNT dispersion with cRODs.

dispersant which simultaneously utilizes three different dispersion mechanisms including surfactant adsorption, polymer wrapping, and charge repulsion to synergistically enhance the dispersion of SWNTs in water. Simultaneous application of the three different dispersion mechanisms is achieved by using polymerized charged rod-like nanoparticles which have hydrophobic cores surrounded by hydrophilic surfaces with controlled surface charge densities (cROD, Fig. 1). Since the cRODs are made of cylindrical micelles encapsulated or wrapped by negatively charged polymers (polymerized counterion chains), the cROD is a perfect candidate for the synergistic SWNT dispersion in water utilizing surfactant self-assembly, polymer wrapping, and electrostatic repulsion, simultaneously. During the dispersion process which includes sonication of the mixture of SWNTs and cRODs in water, the cRODs may be temporarily disintegrated or deformed by sonication or contact interaction with SWNTs and re-assemble on the surface of exfoliated SWNTs, resulting in the two possible stable encapsulation structures (Fig. 1). The cROD assisted dispersion of SWNTs in water has been characterized by UV-vis-NIR spectroscopy, zeta potential measurement, atomic force microscopy and small-angle neutron scattering techniques. To our knowledge, this is the first demonstration of SWNT dispersion in water using polymerized charged rod-like nanoparticles which provide three different dispersion mechanisms, surfactant adsorption, polymer wrapping and charge repulsion, simultaneously.

## 2. Results and Discussion

Charged rod-like nanoparticles with controlled surface charge density (cROD) are fabricated by free radical polymerization of the 4-vinylbenzoate counterions of cetyltrimethylammonium 4-vinylbenzoate (CTVB) worm-like micelles in the presence of varying amounts of sodium 4-styrenesulfonate (NaSS) in water. The surface charge of the $cROD_x$, where $x$ stands for the NaSS mol % relative to the CTVB concentration, is controlled by the NaSS co-monomer concentration (0, 5, 15, 25, and 40 mol % relative to the CTVB concentration for $x = 0$, 5, 15, 25, and 40, respectively) during the polymerization, thus overcharging the micelles by incorporating polymerizable anions ($SS^-$). The surface charge densities (zeta potentials) and structures of the $cROD_x$ have been reported in a previous study.[28] In that study, the zeta potential of the $cROD_x$ changed monotonically from positive (13 mV) to negative (−44 mV) as the concentration of NaSS was increased from 0 to 40 mol %. The small angle neutron scattering (SANS) measurements showed that the $cROD_x$ are stable cylindrical nanoparticles whose diameter is constant at 4 nm. The length of the $cROD_x$ initially increases (from 44 nm when $x = 0$) with $x$, and after reaching a maximum (85 nm when $x = 5$ where the surface charge is nearly neutral), it decreases (to 20 nm when $x = 40$). The $cROD_x$ assisted dispersions of SWNT ($cROD_x$-SWNT) are obtained by sonicating mixtures of $cROD_x$ and SWNTs in $D_2O$. To precipitate bundled SWNTs and obtain individually isolated $cROD_x$-SWNTs, the dispersions are ultracentrifuged, and decanted solutions are used for further characterization.

The ultra-centrifuged and decanted $cROD_x$-SWNT mixtures in $D_2O$ did not show any visible aggregates. While the $cROD_x$-SWNT (with $x = 0$, 5) dispersions are translucent ($x = 0$) and almost transparent ($x = 5$), indicating low concentrations of SWNTs, the $cROD_x$-SWNT (with $x = 15$, 25, and 40) dispersions are dark black, indicating high concentrations of SWNTs (Fig. 2a). The $cROD_0$-SWNT, which has a low SWNT concentration, starts to show sludge-like aggregates after a few days, while all others are stable for more than 8 months. This indicates that the dispersion power of $cROD_x$ and the dispersion stability of $cROD_x$-SWNT are strongly correlated with the surface charge densities of particles, as expected. The UV-vis-NIR spectra of all the $cROD_x$-SWNT dispersions (except the $cROD_5$-SWNT in which the SWNT concentration is too low for measurement) show sharp van Hove transition peaks, indicating the presence of individually isolated SWNTs[14] (Fig. 2b). The SWNT concentrations estimated from the UV-vis NIR intensities at 744 nm using Beer's law are 77 mg $L^{-1}$, ~0 mg $L^{-1}$, 437 mg $L^{-1}$, 292 mg $L^{-1}$,

ADVANCED FUNCTIONAL MATERIALS



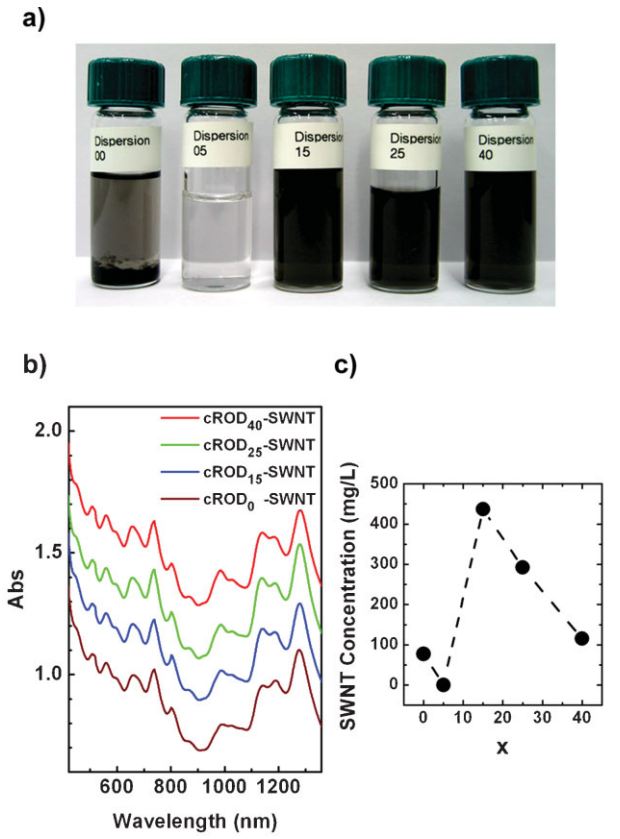


**Figure 2.** a) Photos of the cROD$_x$-SWNT dispersion in water where $x$ stands for the NaSS mol % relative to the CTVB concentration. The numbers in the photos are $x$. b) UV-vis-NIR spectra of the cROD$_x$-SWNT dispersions in water. The spectra are normalized to 1 at 744 nm and shifted vertically for visual clarity. c) SWNT concentration in the cROD$_x$-SWNT dispersions in water determined from UV-vis-NIR spectra. The dashed line is a guide for the eye.

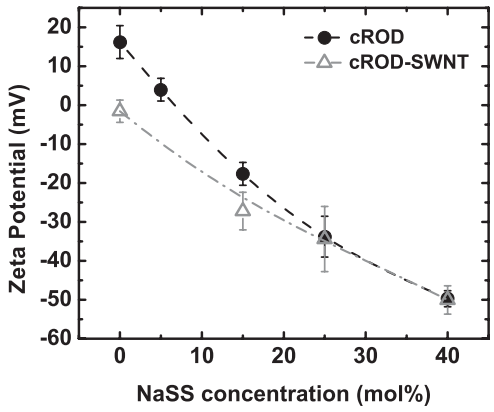


**Figure 3.** Zeta potentials of cROD$_x$ and cROD$_x$-SWNT in water. The dashed line (cROD) and dash-dotted line (cROD$_x$-SWNT) are guides for the eye.

and 115 mg L$^{-1}$ for cROD$_x$-SWNT with $x = 0$, 5, 15, 25, and 40, respectively (Fig. 2c).

In general, the stability of colloidal particles is greatly affected by their surface charge density. Therefore, the zeta potentials of cROD$_x$ and cROD$_x$-SWNT with $x = 0$, 5, 15, 25, and 40 were measured to understand the effects of surface charge on the dispersion. The zeta potential of cROD$_x$ ($x = 0$, 5, 15, 25, and 40; 0.5 wt %) in $D_2O$ are 16.2 mV, 4.0 mV, −17.7 mV, −33.8 mV, and −49.7 mV, respectively, which is consistent with previous results.[28] The ultra-centrifuged and decanted cROD$_x$-SWNTs exhibit negative shifts of zeta potentials compared to the cROD$_x$ (Fig. 3). The negative shift of zeta potentials can be attributed to the negative surface charges of pristine SWNTs in aqueous solution.[29–31] Although the zeta potentials of the anisotropic particles obtained by Smoluchowski's equation may be underestimated,[32] they are still useful to qualitatively understand the effects of the surface charge of the cROD$_x$-SWNTs on the dispersion. As expected, the poorest quality dispersions occur when the magnitude of the zeta potential of cROD$_x$-SWNT is near zero.

To test the re-dispersibility of the cROD$_x$-SWNT in water, powders of cROD$_x$-SWNT were prepared by freeze-drying the cROD$_x$-SWNT dispersions. The powders are dispersed in water by 10 minutes of vortex mixing at the same SWNT concentrations as before freeze-drying (77 mg L$^{-1}$, 437 mg L$^{-1}$, 292 mg L$^{-1}$, and 115 mg L$^{-1}$ for $x = 0$, 15, 25, and 40, respectively) (Supporting Information, **Fig. S1a**). For more than 8 months, no visible aggregates are found in the re-dispersed solutions of cROD$_x$-SWNTs with the NaSS concentration greater than 15 mol % ($x = 15$, 25, and 40). On the other hand, the cROD$_0$-SWNT exhibits sludge-like aggregates immediately after the re-dispersion, as expected. This confirms the contribution of Coulomb repulsive interactions to the stability of SWNT dispersions. For all the cROD$_x$-SWNT re-dispersed in water, the UV-vis-NIR spectra are practically identical with the spectra of the dispersions before freeze drying, showing sharp van Hove transition peaks (Supporting Information, Fig. S1b). Considering that the van Hove transition peaks of bundled SWNTs are weakened or flattened when the electronic structures of SWNTs are disrupted by bundling,[14] it is interesting to see that the poorly re-dispersed cROD$_0$-SWNT still shows sharp van Hove transition peaks. This may indicate that the sludge-like aggregates of cROD$_0$-SWNTs are aggregated networks of mostly isolated SWNTs rather than tightly bundled SWNTs.

To understand the encapsulation structures of cROD$_x$-SWNTs, atomic force microscopy (AFM) measurements were performed for cROD$_{15}$-SWNTs which showed the highest concentration of SWNT in this study. For AFM measurements, samples were prepared by spin-coating the cROD$_{15}$-SWNT dispersion on Si wafers. The diameter distribution of bare SWNTs (calcined cROD$_{15}$-SWNTs) is sharply peaked with a mean value of (1.03 ± 0.22) nm, indicating that most of the cROD$_{15}$-SWNTs are dispersed in an isolated form (Fig. 4a). The AFM images of cROD$_{15}$-SWNTs (without calcination) show a relatively wider diameter distribution, ranging from 1 nm to 5 nm (Fig. 4b). Since the diameter distribution of bare SWNTs is sharply peaked at 1.03 nm, the wider diameter

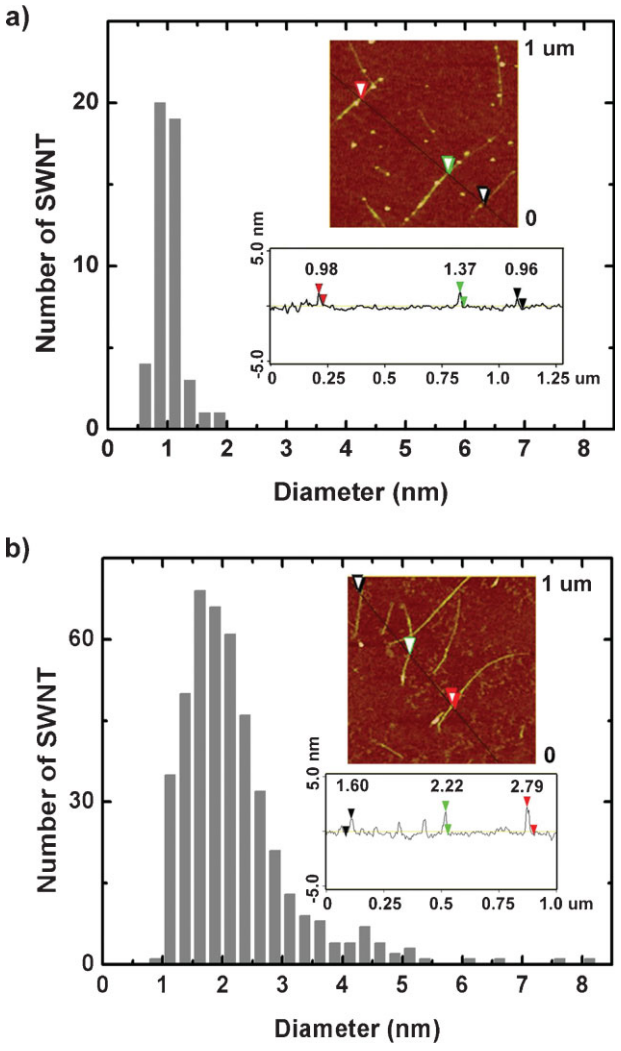


**Figure 4.** AFM analyses of $cROD_{15}$-SWNT a) with and b) without calcination at 300 °C.

distribution of $cROD_{15}$-SWNTs can be attributed to a wide distribution of the encapsulating shell thickness. For simplicity, the distribution of encapsulating shell thickness is obtained by subtracting the mean diameter of bare SWNTs from the diameter distribution of $cROD_{15}$-SWNTs. This shell thickness distribution is well fitted with a Schulz distribution function, resulting in a mean shell thickness of $(0.57 \pm 0.01)$ nm and polydispersity of $(0.64 \pm 0.01)$, where the polydispersity ($\sigma/t$) is defined with the variance of the shell thickness ($\sigma^2$) and the number-averaged shell thickness ($t$).

From the shell thickness distribution, the encapsulation structure of $cROD_{15}$-SWNT can be understood as follows. Since the diameters of SWNT and $cROD_{15}$ are 1 nm and 4 nm, respectively, if an isolated SWNT is inserted into the core of $cROD_{15}$ (cylindrical encapsulation as depicted in Fig. 1a), the diameter of $cROD_{15}$-SWNTs should be 5 nm with an encapsulating shell thickness of 2 nm. The measured shell thickness distribution has, however, a mean value of $(0.57 \pm 0.01)$ nm which is much smaller than 2 nm. Therefore, the cylindrical encapsulation is not the dominant encapsulation structure of $cROD_{15}$-SWNT, although it can not be completely ruled out because some of $cROD_{15}$-SWNTs show shell thickness of about 2 nm. Another possible encapsulation structure is a surfactant assisted polymeric wrapping as schematically described in Fig. 1b. The driving force of the polymeric wrapping of $cROD_{15}$-SWNT can be attributed to the π-π stacking interaction of the aromatic groups of the polymerized counterion chains with SWNTs as it is for DNA[33] or conjugated polymer assisted SWNT[11,19] dispersions. Once the negatively charged polymerized counterion chains are wrapped around the SWNTs, the surfactants ($CTA^+$) with positively charged head groups are driven to attach to the polymeric chains by Coulomb attraction, providing additional coverage of the SWNT surfaces and increasing the integrity of the polymeric wrapping. In this surfactant assisted polymeric wrapping of SWNTs, the shell thickness is expected to be smaller than 2 nm and have a rather broad distribution, which agrees with the AFM results. This suggests that while a small fraction of SWNTs may be encapsulated by the cylindrical micellar sheath (Fig. 1a), the majority of the dispersed SWNTs are encapsulated by surfactant assisted polymeric wrapping (Fig. 1b).

The encapsulation structure of $cROD_{15}$-SWNT is in contrast with the SWNTs which are stabilized by in-situ polymerization of CTVB micelles (p-SWNTs) in water.[16] In this in-situ polymerization method, the mixture of CTVBs and SWNTs was free radical polymerized after sonication. It was shown that the p-SWNTs have cylindrical encapsulation structures where each SWNT is surrounded by a cylindrical micelle whose outer surface is wrapped by polymerized counterion chains, resulting in a well defined shell thickness of 2 nm (as Fig. 1b). This structural difference between the cROD-SWNTs and the p-SWNTs can be explained as follows. In the case of the p-SWNTs, a cylindrical surfactant monolayer is formed on the surface of an isolated SWNT and the counterions, which reside near the outer hydrophillic surface of the encapsulating micelle, are polymerized to lock in the cylindrical surfactant monolayer. Here, the π-π stacking interaction between the polymerized counterion chains and the SWNTs are minimized by the presence of an adsorbed surfactant layer. On the other hand, in the $cROD_x$-SWNTs, the $cROD_x$ has already been polymerized, and it is more likely that the aromatic polymer chain at the surface of the micelle may be attached to the surface of SWNTs by π-π stacking and deformed into the surfactant assisted polymeric wrapping structure. Once the polymeric wrapping structure is formed, it would be energetically difficult for the polymer backbone of the cRODs to reassemble into the original cylindrical micellar structure due to the collective π-π stacking and wrapping of the polymerized counterion chains around the SWNTs.

To understand the in-situ encapsulation structures of the $cROD_x$-SWNTs in water, SANS measurements were performed on the ultracentrifuged and decanted $cROD_x$-SWNTs and $cROD_x$s alone ($x = 15$, 25, and 40) in $D_2O$ using the NG3

ADVANCED FUNCTIONAL MATERIALS



30 m SANS instrument at NIST in Gaithersburg, MD. In the case of the $cROD_x$ alone in $D_2O$, as the NaSS concentration increases from 15 mol % to 40 mol %, the scattering intensities in the low q region decrease due to the increased Coulomb repulsive interactions but the scattering intensities in the high $q$ region do not change (Fig. 5a) ($q > 0.03$ Å$^{-1}$; $q = (4\pi/\lambda)\sin(\theta/2)$, $\lambda$ is the neutron wavelength, and $\theta$ is the scattering angle). Considering that the diameter of all the $cROD_x$ are identical at 4 nm, this indicates that, in the high q region above $q = 0.03$ Å$^{-1}$, the scattering intensities are mainly determined by the form factor (the intra-particle interference) of the dispersed particles with negligible influence of the inter-particle interactions. In the case of the $cROD_x$-SWNTs in $D_2O$, the scattering intensities show similar behavior as that of the $cROD_x$ except small changes around $q = 0.07$ Å$^{-1}$ (Fig. 5b). The small changes around $q = 0.07$ Å$^{-1}$ can be attributed to the difference in the SWNT concentrations rather than the effects of the inter-particle interactions. It should be noted that the slopes of scattering intensities of the $cROD_x$-SWNTs in the low q region are steeper (but still lower than $q^{-1}$) than those of the corresponding $cROD_x$, which indicates the existence of well dispersed isolated SWNTs.[34]

As a representative analysis, a model fit of the scattered intensity of the $cROD_{15}$-SWNT and the $cROD_{15}$ alone in $D_2O$ is presented (Fig. 6). Since the structure factor (inter-particle interference) for highly anisotropic particles such as SWNTs is not easily calculated, the analysis of the measured SANS intensities over the full $q$-range is problematic. However, since the effects of the structure factor in the high $q$ region is negligible, the form factor analyses are performed only in the high q region above $q = 0.03$ Å$^{-1}$ where all the information for the cross sectional structures of thin cylindrical particles is contained. In this analysis, the neutron scattering length densities of SWNT ($4.9 \times 10^{-6}$ Å$^{-2}$), CTVB ($0.35 \times 10^{-6}$ Å$^{-2}$), and $D_2O$ ($6.33 \times 10^{-6}$ Å$^{-2}$) are used. The scattering intensity of the $cROD_{15}$ alone in $D_2O$ was analyzed using the cylindrical form factor resulting in a radius of ($1.97 \pm 0.01$) nm which is consistent with the stretched chain length of CTVB (2.18 nm). Here, the length of the $cROD_{15}$ was fixed at 42 nm which was determined in a previous study.[28] The difference between the simulated curve (dotted line) and the scattering intensity of $cROD_{15}$ in the low q region is due to the Coulomb repulsive interaction mentioned above.

The $cROD_{15}$-SWNT dispersion, which may contain free $cROD_{15}$ not involved in the wrapping of SWNTs, was modeled by a sum of a cylindrical form factor and a core-shell cylindrical form factor representing the free $cROD_{15}$

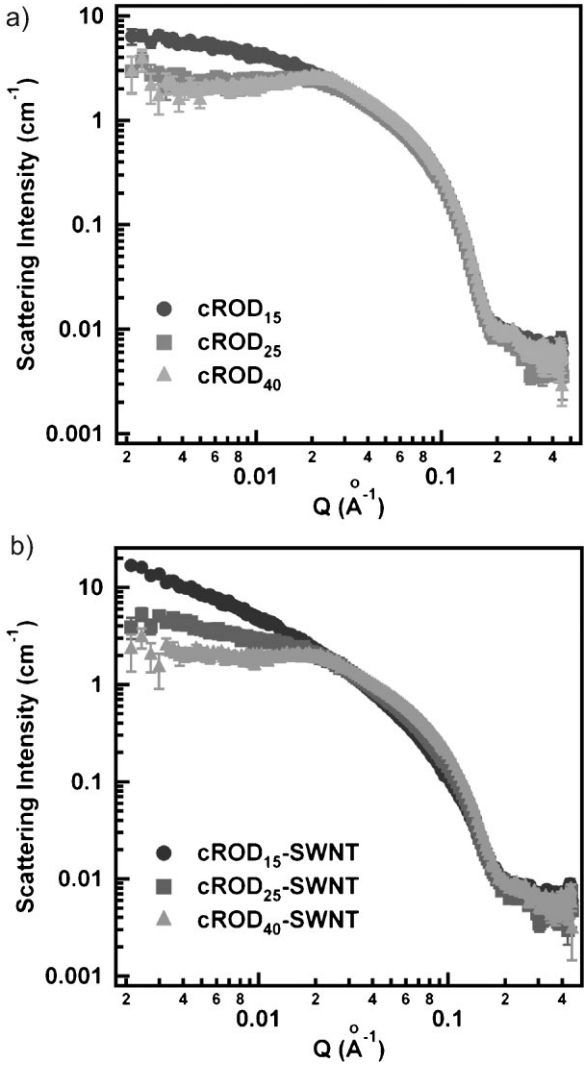


**Figure 5.** SANS intensities of a) $cROD_x$ (0.5 wt %) and b) $cROD_x$-SWNT in $D_2O$ ($x = 15$, 25, and 40). The concentrations of SWNTs in the $cROD_x$-SWNT dispersions are 437 mg L$^{-1}$, 292 mg L$^{-1}$, and 115 mg L$^{-1}$ for $x = 15$, 25, and 40, respectively.

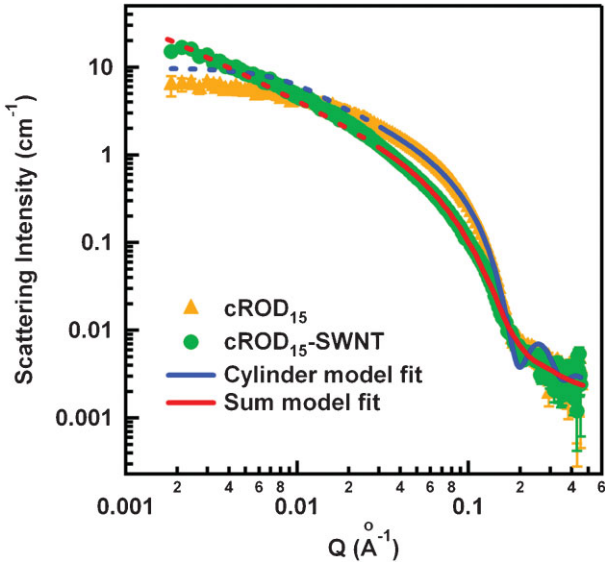


**Figure 6.** SANS intensities and model calculations of $cROD_{15}$ and $cROD_{15}$-SWNT in $D_2O$. Model fits have been performed in the high q-region only ($q > 0.03$ Å$^{-1}$, solid lines). The dotted lines indicate simulated form factors with fitted variables.

and the $cROD_{15}$-SWNT, respectively. The scattered intensity of the $cROD_{15}$-SWNT dispersion, therefore, can be described as $I(q) = \varphi_{free-cROD} P_{cyl}(q)/v_{free-cROD} + \varphi_{cROD-SWNT} P_{core-shell}(q)/v_{cRod-SWNT} + b$, where $P_{cyl}(q)$ is the cylindrical form factor, $P_{core-shell}(q)$ is the core-shell cylindrical form factor, $\varphi_{free-cROD}$ is the volume fraction of free $cROD_{15}$ and $v_{free-cROD}$ is the volume of a single free $cROD_{15}$, $\varphi_{cROD-SWNT}$ is the volume fraction of $cROD_{15}$-SWNT and $v_{cROD-SWNT}$ is the volume of a single $cROD_{15}$-SWNT, and $b$ is the incoherent scattering. In this analysis, the dimensions for the $cROD_{15}$ were fixed at the values determined from the analysis of the $cROD_{15}$. To represent the $cROD_{15}$-SWNT, the core radius and length of the core-shell cylinder were fixed at 0.5 nm and 500 nm, respectively (both are estimated from AFM images). Since the AFM results show a broad encapsulation thickness distribution of the $cROD_{15}$-SWNTs which is well fitted with a Schulz distribution function with a polydispersity of 0.64, a Schulz distribution function with the same polydispersity was used for the shell thickness of the core-shell cylinder. The summed model fit agrees well with the scattering intensity of the $cROD_{15}$-SWNT dispersion, resulting in an average shell thickness of 0.87 nm. The volume fractions of the residual $cROD_{15}$ and the $cROD_{15}$-SWNTs were 0.00031 and 0.0034. While the volume fraction of the residual $cROD_{15}$ was fitted, the volume fraction of the $cROD_{15}$-SWNTs was calculated from the concentration of bare SWNTs (estimated from the UV-vis NIR spectrum) and the average shell volume. The average shell thickness determined from the scattering intensity is 0.3 nm larger than the value (0.57 nm) obtained from the AFM measurements. Considering that the scattering measurements were performed in an aqueous solution while the AFM images were taken in a dried state, this difference is understandable. Therefore, the encapsulation structure of the $cROD_{15}$-SWNT can be described as a surfactant assisted polymeric wrapping as depicted in Figure 1b.

## 3. Conclusions

A new dispersant for stabilizing SWNTs in water that simultaneously utilizes three different stabilization mechanisms including surfactant adsorption, polymeric wrapping and Coulomb repulsive interaction, has been demonstrated. The new dispersants, charged rod-like nanoparticles (cRODs), are fabricated by free radical polymerization of CTVB micelles in the presence of additional NaSS in water. While the $cROD_x$ with neutral or low surface charge densities ($x = 0, 5$) result in very low SWNT dispersion power and poor stability, the $cROD_x$ with higher surface charge densities ($x = 15, 25, 40$) show good homogeneous dispersions and long term stability. The AFM and SANS measurements show that the encapsulation structure of $cROD_x$-SWNT can be described as surfactant assisted polymeric wrapping where surfactant adsorption and polymeric wrapping work synergistically. The $cROD_x$-SWNTs ($x = 15, 25, 40$) can be fully dried and easily re-dispersed in water, providing enhanced processibility of SWNTs.

## 4. Experiments

*Polymerized Rod-like Micelles with Controlled Surface Charge Density*: Cetyltrimethylammonium 4-vinylbenzoate (CTVB) was synthesized following the method described elsewhere [35]. Sodium 4-styrenesulfonate (NaSS) and $D_2O$ (99.9 mol % deuterium enriched) were purchased from Fluka and Cambridge Isotope Laboratory, respectively. The water-soluble free-radical initiator VA-044 (2,2′-azobis[2-(2-imidazolin-2-yl)propane] dihydrochloride) was purchased from Wako Chemicals. CTVB solutions (1 wt % in $D_2O$) with varying amounts (0, 5, 15, 25, and 40 mol % relative to the CTVB concentration) of NaSS were prepared, which form charged worm-like micelles [28]. To remove residual oxygen, $D_2O$ was bubbled with ultrahigh purity nitrogen gas before use. At 60 °C, 5 mol % (relative to the CTVB concentration) of the initiator VA-044 was injected into the CTVB/NaSS solution. Immediately after the injection of initiator, the CTVB/NaSS solution was vigorously shaken and then put into a thermal bath at 60 °C for about 12 hours until the polymerization process was completed. This resulted in solutions of stable polymerized rod-like nanoparticles with controlled surface charge density depending on the concentration of NaSS.

*Dispersion of SWNTs with Charged Rod-Like Nano Particles*: Super-purified HiPco SWNTs (high-pressure CO conversion type, purity > 98 wt %) were purchased from Carbon Nanotechnologies Inc. The SWNTs were mixed with $cROD_x$ ($x = 0, 5, 15, 25$, and 40; $x$ is NaSS mol % relative to CTVB) in $D_2O$ (2.2 mg $mL^{-1}$ of SWNTs and 5.5 mg $mL^{-1}$ of $cROD_x$), followed by sonication (Cole-Parmer VCX750, 20 kHz, 20 W) for one hour at room temperature. To separate the individually isolated SWNTs from the bundled ones, the sonicated mixture was ultra-centrifuged (ca. 111000 *g*) for 4 hours, and the supernatant (ca. 70%) of the solution was decanted [14]. Some of the decanted SWNT solutions were freeze-dried at −55 °C, resulting in black powders of $cROD_x$-SWNTs.

*Zeta Potential Measurements*: The surface charge densities of polymerized CTVBs and dispersed SWNTs with different amounts of NaSS ($cROD_x$ and $cROD_x$-SWNT respectively) were characterized by zeta potential measurements using a Zeta Plus zeta potential analyzer (Brookhaven Instruments Corporation). The zeta potential was calculated by Smoluchowski's equation via the measurement of the electrophoretic mobility [32]. Zeta potentials of $cROD_x$-SWNTs were measured after diluting samples to SWNT concentrations of 30 mg $L^{-1}$ for detectable signals to be acquired, because SWNTs absorb most of the light leaving no detectable signals when the dispersion is not diluted. For zeta potential measurements of $cROD_x$, samples were prepared at 0.5 wt % particles in $D_2O$.

*UV-vis-NIR Measurements of SWNT Dispersions*: A Jasco V-570 UV-vis-NIR spectrometer with quartz cells of 2 mm beam path length was used to characterize the quality of SWNT dispersions and estimate the concentrations of SWNTs in the dispersions. SWNT dispersions at very low concentrations (0.05–0.25 mg $mL^{-1}$) were prepared by sonicating a mixture of SWNTs and $cROD_0$ (1.1 mg $mL^{-1}$) in $D_2O$ for 1 hour. Assuming that at such low concentrations, all SWNTs are fully dispersed and contribute to the UV-vis-NIR intensity at 744 nm (where the UV spectra from $cROD_x$ do not interfere), these low concentration samples were used as calibration to estimate the concentration of SWNTs in solution [36]. The extinction coefficient estimated from the UV-vis NIR measurements of the reference samples is 32 mL $mg^{-1}$ $cm^{-1}$ at 744 nm, which is comparable to the extinction coefficient reported elsewhere [37–39]. Using the extinction coefficient obtained above, the concentrations of SWNTs in solutions were calculated from Beer's Law, $A = \varepsilon L c$, where $A$, $\varepsilon$, $L$, and $c$ are absorbance, extinction coefficient, beam path length, and concentration of absorbers, respectively.

*Atomic Force Microscope (AFM) Measurements*: The AFM images were taken in tapping mode by using a VEECO AFM instrument (Nanoman, SECPM). The $cROD_x$-SWNT solution was spin-coated at 4000 rpm for 1.5 min onto freshly cleaned silicon wafers. Some of the samples were baked at 300 °C for 4 hours to remove

ADVANCED FUNCTIONAL MATERIALS



$cROD_x$ resulting in bare SWNTs. NanoScope® III imaging and analysis software (Digital Instruments) was used to estimate the diameter distributions of bare SWNTs or $cROD_x$-SWNT from AFM images.

*Small Angle Neutron Scattering (SANS) Measurements*: Neutron scattering experiments were performed on the NG3 30m SANS instrument at the National Institute of Standards and Technology (NIST) Center for Neutron Research in Gaithersburg, MD. Neutrons of wavelength $\lambda = 6$ Å and $\lambda = 8.4$ Å with full width at half-maximum $\Delta\lambda/\lambda = 14\%$ were used. Three different sample-to-detector distances (SDD = 1.3 m and 4 m for $\lambda = 6$ Å, and SDD = 13.2 m for $\lambda = 8.4$ Å with a set of refractive focusing lenses [40]) were used to cover q range of $0.001\ \text{Å}^{-1} < q < 0.45\ \text{Å}^{-1}$ where $q = (4\pi/\lambda)\sin(\theta/2)$ is the magnitude of the scattering vector with $\theta$ being the scattering angle. All the samples were contained in quartz cells of 2 mm path length. Sample scattering was corrected for background and empty cell scattering, and the sensitivity of individual detector pixels. The corrected data sets were circularly averaged and placed on an absolute scale using software supplied by NIST [41] through a direct beam flux method.

Received: March 3, 2008
Revised: May 3, 2008
Published online: September 1, 2008

[1] R. Saito, G. Dresselhaus, M. S. Dresselhaus, *Physical Properties of Carbon Nanotubes*, Imperial College Press, London **1998**.
[2] M. S. Dresselhaus, G. Dresselhaus, P. Avouris, *Carbon Nanotubes Syhthesis, Structure, Properties, and Applications*, Springer, New York **2003**.
[3] P. Harris, *Carbon Nanotubes and Related Structures*, Cambridge University Press, Cambridge, UK **1999**.
[4] S. J. Tans, A. R. Verschueren, C. Dekker, *Nature* **1998**, *393*, 49.
[5] S. J. Kang, C. Kocabas, T. Ozel, M. Shim, N. Pimparkar, M. A. Alam, S. V. Rotkin, J. A. Rogers, *Nat. Nanotechnol.* **2007**, *2*, 230.
[6] J.-P. Cleuziou, W. Wernsdorfer, V. Bouchiat, T. Ondarcuhu, M. Monthioux, *Nat. Nanotechnol.* **2006**, *1*, 53.
[7] P. W. Barone, S. Baik, D. A. Heller, M. S. Strano, *Nat. Mater.* **2004**, *4*, 86.
[8] Z. Liu, W. Cai, L. He, N. Nakayama, K. Chen, X. Sun, X. Chen, H. Dai, *Nat. Nanotechnol.* **2007**, *2*, 47.
[9] P. M. Ajayan, L. S. Schadler, C. Giannaris, A. Rubio, *Adv. Mater.* **2000**, *12*, 750.
[10] J. N. Coleman, U. Khan, Y. K. Gun'ko, *Adv. Mater.* **2006**, *18*, 689.
[11] M. J. O'Connell, P. Boul, L. M. Ericson, C. Huffman, Y. Wang, E. Haroz, C. Kuper, J. Tour, K. D. Ausman, R. E. Smalley, *Chem. Phys. Lett.* **2001**, *342*, 265.
[12] J. Hilding, E. A. Grulke, Z. G. Zhang, F. Lockwood, *J. Dispersion Sci. Technol.* **2003**, *24*, 1.
[13] L. A. Girifalco, M. Hodak, R. S. Lee, *Phys. Rev. B* **2000**, *62*, 13104.
[14] M. J. O'Connell, S. M. Bachilo, C. B. Huffman, V. C. Moore, M. S. Strano, E. H. Haroz, K. L. Rialon, P. J. Boul, W. H. Noon, C. Kittrell, J. Ma, R. H. Hauge, R. B. Weisman, R. E. Smalley, *Science* **2002**, *297*, 593.
[15] D. Tasis, N. Tagmatarchis, V. Georgakilas, M. Prato, *Chem. Eur. J.* **2003**, *9*, 4000.
[16] V. C. Moore, M. S. Strano, E. H. Haroz, R. H. Hauge, R. E. Smalley, J. Schmidt, Y. Talmon, *Nano Lett.* **2003**, *3*, 1379.
[17] T.-H. Kim, C. Doe, S. R. Kline, S.-M. Choi, *Adv. Mater.* **2007**, *19*, 929.
[18] B. Z. Tang, H. Xu, *Macromolecules* **1999**, *32*, 2569.
[19] S. Qin, D. Qin, W. T. Ford, J. E. Herrera, D. E. Resasco, S. M. Bachilo, R. B. Weisman, *Macromolecules* **2004**, *37*, 3965.
[20] Y. Dror, W. Pyckhout-Hintzen, Y. Cohen, *Macromolecules* **2005**, *38*, 7828.
[21] C. Richard, F. Balavoine, P. Schultz, T. W. Ebbesen, C. Mioskowski, *Science* **2003**, *300*, 775.
[22] Y. Wu, J. S. Hudson, Q. Lu, J. M. Moore, A. S. Mount, A. M. Rao, E. Alexov, P. C. Ke, *J. Phys. Chem. B* **2006**, *110*, 2475.
[23] R. Qiao, P. C. Ke, *J. Am. Chem. Soc.* **2006**, *128*, 13656.
[24] M. Zheng, A. Jagota, E. D. Semke, B. A. Diner, R. S. Mclean, S. R. Lustig, R. E. Richardson, N. G. Tassi, *Nat. Mater.* **2003**, *2*, 338.
[25] S. Badaire, C. Zakri, M. Maugey, A. Derré, J. N. Barisci, G. Wallace, P. Poulin, *Adv. Mater.* **2005**, *17*, 1673.
[26] T. J. Simmons, D. Hashim, R. Vajtai, P. M. Ajayan, *J. Am. Chem. Soc.* **2007**, *129*, 10088.
[27] L. H. Torn, A. d, Keizer, L. K. Koopal, J. Lyklema, *Colloids Surf. A* **1999**, *160*, 237.
[28] T.-H. Kim, S.-M. Choi, S. R. Kline, *Langmuir* **2006**, *22*, 2844.
[29] M. Sano, J. Okamura, S. Shinkai, *Langmuir* **2001**, *17*, 7172.
[30] L. Jiang, L. gao, J. Sun, *J. Colloid Interface Sci.* **2003**, *260*, 89.
[31] L. Vaisman, G. Marom, H. D. Wagner, *Adv. Funct. Mater.* **2006**, *16*, 357.
[32] R. J. Hunter, *Zeta Potential in Colloid Science*, Academic, London **1981**.
[33] R. R. Johnson, A. T. C. Johnson, M. L. Klein, *Nano Lett.* **2008**, *8*, 69.
[34] W. Zhou, M. F. Islam, H. Wang, D. L. Ho, A. G. Yodh, K. I. Winey, J. E. Fischer, *Chem. Phys. Lett.* **2004**, *384*, 185.
[35] S. R. Kline, *Langmuir* **1999**, *15*, 2726.
[36] W. Wenseleers, I. I. Vlasov, E. Goovaerts, E. D. Obraztsova, A. S. Lobach, A. Bouwen, *Adv. Funct. Mater.* **2004**, *14*, 1105.
[37] S. H. Jeong, K. K. Kim, S. J. Jeong, K. H. An, S. H. Lee, Y. H. Lee, *Synth. Met.* **2007**, *157*, 570.
[38] A. N. G. Parra-Vasquez, I. Stepanek, V. A. Davis, V. C. Moore, E. H. Haroz, J. Shaver, R. H. Hauge, R. E. Smalley, M. Pasquali, *Macromolecules* **2007**, *40*, 4043.
[39] V. C. Moore, Ph. D. Thesis, Rice University **2005**.
[40] S. M. Choi, J. G. Barker, C. J. Glinka, H. T. Cheng, P. L. Gammel, *J. Appl. Crystallogr.* **2000**, *33*, 793.
[41] S. R. Kline, *J. Appl. Crystallogr.* **2006**, *39*, 895.

  